Detection of Energetic Heavy Ions

Robert Katz
University of Nebraska-Lincoln, rkatz2@unl.edu

S. C. Sharma
University of Nebraska-Lincoln, sharma@uta.edu

Mehdi Homayoonfar
University of Nebraska-Lincoln

Detection of Energetic Heavy Ions

R. Katz, S. C. Sharma, and M. Homayoonfar

Behlen Laboratory of Physics, University of Nebraska–Lincoln, Lincoln, Nebraska 68508, U.S.A.

Abstract

The delta-ray theory of track structure, applied earlier to such 1-or-more hit detection systems as the inactivation of dry enzymes and viruses, the NaI(Tl) scintillation counter, and nuclear emulsion, is extended to the silver activated phosphate glass dosimeter, the LiF thermoluminescent dosimeter, the creation of free radicals in solid biological substances, solid and liquid organic scintillators, and the ferrous sulfate (Fricke) dosimeter. The response of these systems to both gamma-rays and heavy ions is characterized by two parameters: 1) D_γ^{37}, the dose of gamma-rays at which 37% of the sensitive elements remain unaffected by the radiation, and 2) a_0, the physical radius (or the exciton diffusion length, or the range of short-range order) of the sensitive element. The decline of detector response with increase in the stopping power of the bombarding ion, and the non-linearity of the detector response are characteristic properties of 1-hit detectors, and are most pronounced for the most sensitive detectors. Explicit information about the cross-sectional area of the sensitive target cannot be gained from measurement of the activation cross-section as a function of the stopping power of the incident ion, for there is no saturation cross-section for 1-hit detectors. Since parameters describing the incident ion and those describing the detector are not separable variables, the response of a detector cannot be described through a product of two factors, one containing only ion parameters and representing "radiation quality," and the other containing only detector parameters and representing " detector quality."

1. Introduction

The response of several detecting systems to energetic heavy ions is related to their response to gamma-rays through the delta-ray theory of track structure, in which the local dose distribution arising from the ejected secondary electrons (delta-rays) about the path of an energetic ion is combined with a gamma-ray dose-response function to predict the response of the detector to heavy ions.

The model has been applied to the survival of bacterial spores, yeast, and mammalian cells after heavy ion irradiation,[1] to the formation of etchable tracks in dielectrics,[2] to the formation of tracks in nuclear emulsion,[3,4] to the response of NaI(Tl) scintillation counters,[5] and to the inactivation of dry enzymes and viruses by heavy ion beams.[6]

In the present work, we show that the model describes the response of the silver activated phosphate glass dosimeter, the LiF thermoluminescent dosimeter, the creation of free radicals in solid biological substances, the response of solid and liquid organic scintillators, and of the ferrous sulfate (Fricke) dosimeter, to energetic heavy ions.

Except for biological cells, whose sensitive element structure is complex and only partly understood, and where the gamma-ray response may be represented by the mathematical form of the many-target single-hit statistics, and for the formation of etchable tracks

in dielectrics,[2,7] where massive damage must be done within a minimal radius of about 20 Å, all detecting systems studied here and in earlier work respond to the local dose of ionizing radiation as 1-or-more hit detectors. By this we mean that one activation event suffices to "turn on" a sensitive element. In Figure 1, the detectors are ordered according to their gamma-ray dose-response characteristics and their sensitivity.

To understand detector response, we take the detector to consist of a set of identical sensitive elements (which may be atomic, or molecular, or collectively acting macroscopic aggregates like the photographic grain) which are sometimes embedded in a passive matrix that may act as an energy transfer medium. We take the initiation of an action in a sensitive element to arise from a single quantized event called a hit,[8] but otherwise unidentified, and take the energy dose deposited by secondary electrons to be a measure of the density of hits.

It is not necessary that the sensitive element has a clear physical boundary. In NaI(Tl),[9] and in liquid scintillators sensitized with PPO (diphenyloxazole),[10] the detector response varies with increasing concentration, x, of the sensitive substance approximately as $1 - e^{-x/x_0}$. We interpret this response to arise from the fraction of the detector volume which is covered by overlapping sensitive volumes, and evaluate the sensitive volume radius, a_0 from the "saturation" value of the concentration, as 35 Å, in NaI(Tl), and 150 Å in liquid scintilla-

```
------------------ ONE-OR-MORE HIT ---------------------    --M-TARGET SINGLE-HIT --   -- MANY HIT --

            EMULSION          DOSIMETERS          SOLID BIOLOGICALS    BIOLOGICAL CELLS        DIELECTRICS
10^10  -                  -                   -                    -                  -          OLIVINE        - 10^10
                                                    *INACTIVATION*

       -            -                 -                 -               -                -           - ‹
                                                                                            MICA
ERG CM^-3                                           LYSOZYME                                             ERG CM^-3
                                                    TRYPSIN                               .
       -            -                 -                 -               -                -           -
                                                    DNA-ASE

10^9   -                  -                   -                    -                  -                         - 10^9
                                                                                         POLYCARBONATE

       -            -                 -                 -               -                -           -
                                                β-GALACTOSIDASE
                                                                                         CELLULOSE  NITRATE
       -            -                 -                 -               -                -           -

10^8   -            -FERROUS SULFATE-DEAER-                          -                -           - 10^8
                                                φX-174 PHAGE
                                                    T-1 PHAGE
       -            - FERROUS SULFATE-AER -             -               -                -           -
                         NaI(Tl)

       -      K-2   -                ‾ *RADICAL PRODUCTION*  ‾           -                -           -

10^7   -            -         LiF    -           TRYPSIN      BACTERIAL SPORES-H₂S -               - 10^7
              K-1                                    CYTIDINE
                                                                BACTERIAL SPORES- N₂
       -            -                 - GLUTATHIONE (red.)  ‾BACTERIAL SPORES- O₂ ‾  -
              K.0            GLASS
       -            -                 -                 -               -                -           -

10^6   -            -                 -           ALANINE       -                -           - 10^6
                                                GLYCINE  (100°K)
                                SOLID ORGANIC
                                SCINTILLATORS
       -            -                 -  GLYCINE  (200°K)  -              -                -           -
              K.2                                            HAPLOID YEAST

       -            -                 -  GLYCINE  (300°K)  -              -                -           -

10^5   -            -                 -                 -               -                -           - 10^5

       -      K.5   -                 -                 -               -                -           -

                                                            T-1 HUMAN KIDNEY-N₂
       -      G.5   -                 -                 - CHINESE HAMSTER -O₂ -          -
                                                            T-1 HUMAN KIDNEY-O₂
                                                                HELA-O₂
10^4   -            -         LIQUID ORGANIC  -                 -               -                - 10^4
                             SCINTILLATORS
```

Figure 1. Radiation detectors. The characteristic dose has different meaning in the different detector categories. For 1-or-more hit detectors it is the dose of gamma-rays at which 37% of the sensitive elements survive, here called D_γ^{37}. This is the largest detector category, including liquid and solid physical,[3,5] chemical, and elementary biological systems.[6] The response of biological cells to gamma-rays is best described by the mathematical form of many-target, single-hit statistics,[1] where the characteristic dose is the dose increment in which the surviving fraction is decreased by 37%, in the high dose region, where a semi-logarithmic plot of surviving fraction versus dose becomes a straight line. In the case of etchable tracks in dielectrics,[2] the critical dose is the minimal dose deposited at a critical radius of about 20 Å, which is required for track observation.

tors. From study of the variation of the response of the Fricke dosimeter with LET (Linear Energy Transfer, or stopping power) we find $a_0 = 60$ Å , as discussed in section 4.

We find the form of the gamma-ray dose-effect relationship for these detectors from Poisson statistics. In a random distribution, the probability that one of a collection of identical statistical cells contains X hits when the average number of hits per cell is A is given as $A^X e^{-A}/X!$. The probability that there are 1-or-more hits per cell is 1 minus the probability that $X = 0$, and is given by the expression $1 - e^{-A}$.

In a system uniformly irradiated with gamma-rays, D_γ^{37} is the dose at which there is an average of 1 hit per sensitive element. If the system is irradiated with gamma-rays to dose D_γ, the average number of hits per sensitive element is D_γ/D_γ^{37}, so that the probability that any one element of the system experiences 1-or-more hits is

$$P = 1 - e^{-D_\gamma/D_\gamma^{37}} \tag{1}$$

The response of a system irradiated with gamma-rays may be described by a single number, namely D_γ^{37}.

Note that we have applied Poisson statistics to a system in which the distribution of events is not uniform, and not random, and yet Equation (1) describes the behavior of many detectors. While the locations of photon interactions in a medium are random, the positions of each set of ionizations arising from a single photon interaction, through the subsequent secondary electrons, is related closely to the initial site. It is not that the ionizations are randomly distributed that lends validity to Equation (1), but rather that the 1-or-more hit test of randomness used by detecting systems is a very weak test of randomness.[11] The fact that the distribution of ionizing events following gamma-ray irradiation is not Poissonian does not bar the use of Equation (1) as an estimate of the number of significant events.

We emphasize that the assumed dose-effect relationship, Equation (1), arises from stochastic considerations. Fluctuations in the hit density generate the dose-response function. The mean value of the energy density, the dose D_γ, provides sufficient knowledge of those aspects of the hit distribution to which the detector is sensitive, just as the mean value of a Poisson distribution is sufficient information from which to determine all of its moments.

When we consider the mean energy to form an ion-pair, in relation to the energy of an incident gamma-ray photon, or that electron interaction cross-sections peak strongly at electron energies between 5 and 50 eV, it is apparent that the effects produced in detecting systems irradiated with gamma-rays arise principally from second and higher generation electrons, rather than from the primary photon interaction.

In a similar way, the delta-ray theory of track structure takes the actions arising from the passage of an energetic ion to be due to secondary and higher generation electrons, rather than from the primary interactions. Although a large fraction of the energy lost by the primary particle is deposited within tens of Angstroms of the ion's path, only a small part of the observed effect is generated there, because of detector saturability, and because of the small number of sensitive elements contained within a cylinder of such small radius. Energy may be carried by delta-rays out to distances of many microns in condensed matter.

To understand track structure, we must first find the spatial distribution of dose about the path of an ion, as deposited in the sensitive volume elements of the detector. We anticipate that these calculations will be compared to measurements of detector response in which the response is averaged over a sufficiently long segment that the "noise" due to fluctuation in delta-ray production is negligible, or in which the response is averaged over a sufficiently large number of particles in short track segments to achieve the same result. We therefore calculate the average dose distribution, which we write as $\bar{E}(z, \beta, t, a_0)$, for it represents the mean energy density delivered to a sensitive element of radius a_0 whose center is at radial distance t from the path of an ion of effective charge number z moving through the detector at speed βc. In order to calculate the probability that a sensitive element is affected by a passing ion, from the gamma-ray dose-effect relation of Equation (1), we first group sensitive elements into sets which lie along isodose contours, as between adjacent cylindrical shells whose axis is the ion's path, and again consider either a sufficiently long shell or many short shells that surround track segments from many ions at a single speed, as may be appropriate. Thus we write that the probability $P(z, \beta, t, a_0)$ that a sensitive element (of radius a_0 whose center is at distance t from the path of an ion of effective charge number z moving at speed βc) is activated by the passing ion is

$$P(z, \beta, t, a_0) = 1 - \exp[-\bar{E}(z, \beta, t, a_0)/D_\gamma^{37}]. \tag{2}$$

In the event that it is possible to measure the spatial distribution of activated elements about the path of a single ion, P is the quantity which can be directly compared to experiment. In nuclear emulsion, P represents the fraction of grains lying between adjacent cylindrical shells which are rendered developable, and so provides the basis for a calculation of the track width, or of the variation of the photographic blackness of the

track width distance from the ion's path, or of the grain count along the path of an energetic proton.[3]

If we can measure only the total effect generated by a single ion, or the effect produced by a beam of ions, we must calculate the interaction cross-section, σ, for comparison with the results of experiment.

Since the activation cross-section is the probability that single ion activates a single sensitive site in a detector containing 1 such site per unit area, the cross section may be found by integrating P over all t, as

$$\sigma(z, \beta, a_0) = \int_0^\infty 2\pi t P(z, \beta, t, a_0)\, dt. \tag{3}$$

From Equations (2) and (3) we note that the response of a detector to heavy ions may be found from the two detector parameters, D_γ^{37} and a_0. We also note that detector parameters and ion parameters are not separable variables. The latter observation implies the impossibility of describing detector response through a product of two factors, one of which represents the "radiation quality" while the other represents the "detector quality."

A beam of ions of stopping power L and fluence F (ions/cm^2) deposits an ion dose $D_i = FL$ in a thin detector. Since the probability that no action takes place in the detector is $e^{-\sigma F}$, the probability that an action is generated is

$$P = 1 - e^{-\sigma F} = 1 - e^{-D_i/L} \tag{4}$$

Equation (4) describes the response of a thin detector to the absorbed dose of heavy ions, as in "track-segment" bombardment.

We take the radiosensitivity, k, of the detector to be the reciprocal of the dose at which there is 37% survival, so that

for gamma-rays: $k_\gamma = (D_\gamma^{37})^{-1}$,   while   (5)

for heavy ions: $k_i = \sigma/L$.   (6)

In radiobiology, the quotient k_i/k_γ bears the name Relative Biological Effectiveness, or

$$\mathrm{RBE} = k_i/k_\gamma = \sigma D_\gamma^{37}/L \tag{7}$$

To calculate the response of thick detectors to stopping ions, of initial kinetic energy T_i and having range R, we integrate the response over the path length to find

$$\bar{\sigma} R = \int_0^R \sigma\, dr = \int_{T_i}^0 \sigma/L\, dT. \tag{8}$$

The total action produced by a stopping particle de-

pends on $\bar{\sigma} R$, just as the action produced in a track segment of length dr depends on σdr.

We represent the average radiosensitivity, $\bar{k}$, for stopping particles as

$$\bar{k} = \bar{\sigma} R/T_i = \bar{\sigma}/\bar{L}, \tag{9}$$

where we implicitly define $\bar{L} = T_i/R$.

The preceding description makes it possible to outline the mathematical structure through which the response of a detector to neutrons may be calculated. We take Y to represent the number of absorbed neutrons per cm^3 of detector volume, D_n to represent the absorbed dose from neutrons, R_{Zi} to represent the range in cm of an ion of atomic number Z and initial kinetic energy T_i, and dN_{Zi}/dT_i to represent the number of secondary charged particles of atomic number Z and initial kinetic energy T_i per unit initial kinetic energy interval, per absorbed neutron per cm^3 of detector, then we may write

$$D_n = Y \sum_Z \sum_{T_i} (\Delta T_i)\, (dN_{Zi}/dT_i)\, T_i\,, \tag{10}$$

while the activation probability P is

$$P = 1 - \exp\left\{ -Y \left[\sum_Z \sum_{T_i} (\Delta T_i)(dN_{Zi}/dT_i)\, \bar{\sigma}_{Zi} R_{Zi} \right] \right\}. \tag{11}$$

Note that in Equation (11), the quantity Y (absorbed neutrons per cm^3) plays a role equivalent to that of F (particles per cm^2) in Equation (4), while the quantity within the braces in Equation (11) (having dimensions of cm^3) plays a role equivalent to that of σ(cm^2) in Equation (4). As we will see, the present work makes it possible to calculate σ for any 1-hit detector from two detector parameters, a_0 and D_γ^{37}. The theory may be applied to predict neutron response when the spectrum of secondary charged particles in the detector from neutron bombardment is known. Work on the problem of neutron detection is presently under way.

Throughout this work we make use of an expression for the effective charge number z, of an ion of atomic number Z, as given by Barkas,[22]

$$z = Z(1 - e^{-125\beta Z^{-2/3}}). \tag{12}$$

We also require a consistent set of values of the stopping power (LET) of protons and heavy ions. Values for protons are taken from three sources. The table of Janni [13] is used for proton energies from 0.1 to 2 MeV. The table of Northcliffe and Schilling[14] is used for proton energies from 2 MeV to 10 MeV. The table of Barkas and Berger [15] is used for proton energies from 10 to 5000 MeV. The stopping power of heavy ions is cal-

culated from that for protons (p) through use of Equation (12) and the stopping power tables, through the relation

$$L(Z, \beta) = L(p, \beta)[z/z_p]^2, \qquad (13)$$

where z_p is the effective charge number of a proton, as given by Equation (12), $L(Z, \beta)$ is the stopping power of the ion of atomic number Z at relative speed β, and $L(p, \beta)$ is the stopping power of a proton at the same speed. At low speeds, where the tables disagree for the value of the stopping power of an ion, this procedure gives values intermediate to the tabulated values. The range R is calculated from L to sufficient accuracy for present purposes.

2. From gamma-rays to heavy ions

As we have seen, the transition from the dose-effect relation for gamma-rays, Equation (1), to the dose-effect relation for heavy ions, Equation (4), is made from the function $\bar{E}(z, \beta, t, a_0)$ which gives the spatial distribution of dose about an ion's path. Since this function is not known experimentally, we calculate it from available information. Basically, the calculation includes a delta-ray distribution formula for initially free electrons (which may be modified in an attempt to take binding energy into account), an assumed angular distribution of the ejected electrons, and information or approximations about electron paths or electron energy dissipation.

In earlier work electrons have been taken as initially free, or as intially bound with a mean binding energy assigned from energy loss theory. Their angular distribution has been assumed to follow from the classical collision between two particles, or to follow the function $\cos^4\theta$, or that all electrons are ejected normally, and so on. The electron's path has been taken to be straight or scattered. Its energy loss has been taken as constant, or as arising from an algorithm whose output is well matched to energy dissipation data. The resulting calculations of the spatial distribution of ionization energy deposited by secondary electrons are remarkably insensitive to assumptions of angular distribution or of energy dissipation.[1] Unless we are interested in events very close to the ion's path, where assumptions about binding energy may play an important role, or in events at distances so far from the ion's path that the radial distance to which the most energetic electrons penetrate is of critical importance, the dose distribution varies as $z^2\beta^{-2}t^{-2}$.

In the present work we follow the calculation of Butts and Katz,[6] where initially free electrons are taken to be ejected normally, to travel in straight lines, and to have constant energy loss. More complex assumptions are not needed at distances appropriate to detectors of interest here. At distances sufficiently close to the ion's path that binding energy might create a problem, there is little contribution to the cross-section. At distances sufficiently far away that the range of the most energetic electron might create a problem, the dose is low, and again, the error made in the calculation of the cross-section may be neglected. Though several different media are involved in the present investigation, all are represented as having the properties of water, for Butts and Katz have shown that density differences again play a small role in the calculation of the cross-section, for there are compensating corrections in the dose distribution and the D_γ^{37} dose which appear in the numerator and the denomenator of the integrand, when both of these quantities are expressed in units of energy per unit volume.

The calculation of Butts and Katz yields the result that the point distribution in dose, $E(z, \beta, t)$, is given by the expression

$$E(z, \beta, t) = \frac{Ne^4}{mc^2} \frac{z^2}{\beta^2} \left[\frac{1}{t^2} - \frac{1}{t\tau} \right], \qquad (14)$$

where N is the number density of electrons in the medium, and τ is the distance to which the most energetic electrons penetrate. As they have shown, Equation (14) also represents the dose $\bar{E}$ delivered to a sensitive volume of radius a_0, at large distances, where $t/a_0 > 3$. Use of Equation (14) to calculate cross-sections is called the point-target approximation, valid where all sensitive elements through which the ion passes are activated, so that the error made in the use of the point-target approximation close to the ion's path is negligible. In language appropriate to particle tracks in emulsion, this is the "track-width" regime. As we will see, calculated values of the cross-section increase uniformly as we pass from the grain-count to the track-width regime, with increasing values of z^2/β^2 of the bombarding ion which forms the track. For 1-hit detectors there is no hint of a plateau at a value of the cross-section corresponding to the cross-sectional area of the sensitive element.

The appearance of the track of a relativistic proton in emulsion gives the deceptive impression that track structure is linear, as shown in Figure 2, for the ion's path seems to be well defined by the string of developed grains, with few grains other than background nearby, except for an occasional isolated delta-ray. The appearance of the track depends on the observer's perception of what is track and what is background, on

the linear scale of the microscope image, and on the microscope depth of focus. The tracks of heavier ions increase regularly in width with an increase in the number (but not in the relative energy spectrum) of delta-rays, say as from the tracks caused by a progression of particles of increasing Z at relativistic speeds. For such particles, the track extends through a substantial volume, when distances are measured in units of a_0. Notice that at values of t where the probability for

activation of a sensitive element varies as t^{-2}, the differential contribution to the cross-section varies as $d(\ln t)$, from Equation (3). In any 1-hit detector, from the track "boundary," say where 30% of the sensitive sites are activated, to distances approaching τ, there are equal contributions to the cross-section from equal decade intervals in t. It is for this reason that the inactivation cross-section of lysozyme, for example, may exceed its geometric cross-section by a factor of 10 or more.[8]
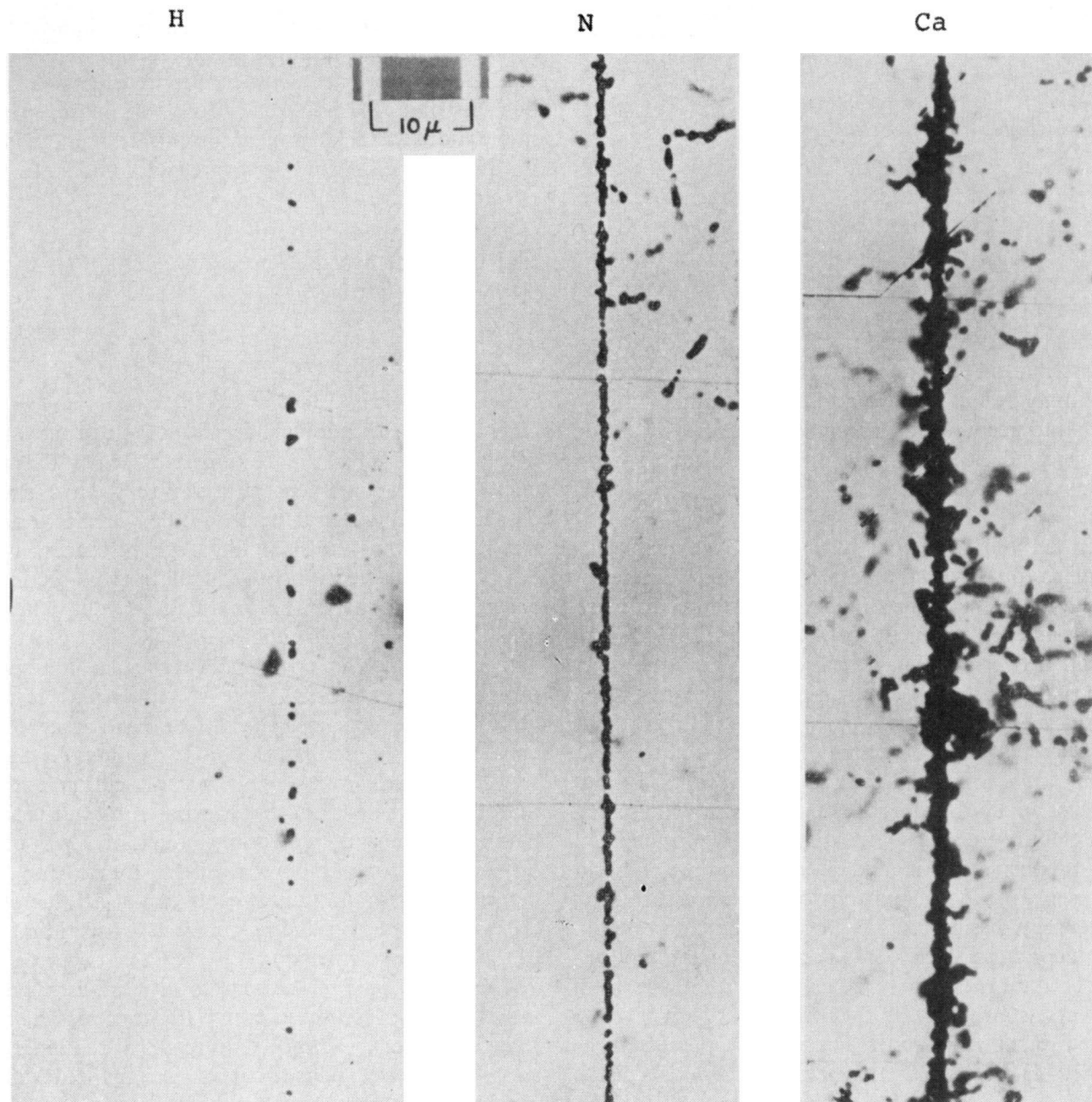
Figure 2. Tracks of relativistic protons, nitrogen, and calcium nuclei in Ilford G.5 emulsion illustrate the grain-count (H), and track-width (Ca) regimes, and the transition between them (N). Courtesy M. M. Shapiro, Naval Research Laboratory.

To incorporate the effect of the size of the sensitive volume, we approximate the sensitive element by a short cylinder of radius a_0 whose axis is parallel to and at distance t from the ion's path.[1,6] By comparison of the results of such dose calculations with earlier work in which spherical averages were used, we conclude that the difference between spherical, cylindrical, and other near spherical volume averages lies in the shape of the shoulder of the curve, near $t/a_0 = 1$, and choose the simpler procedure here, for we have no basis for a more complex choice.

The dose $\bar{E}$ in a short cylinder of radius a_0, whose axis is parallel to and at distance t from the path of an energetic ion, is shown in Figure 3, where $\bar{E}(z, \beta, a_0)\beta^2/z^2$ is plotted against t, for $\beta = 0.05$, 0.15, and 0.99, and for $a_0 = 10^{-7}$ to 10^{-4} cm. To distances where t and a_0 are both substantially less than τ, the values of the plotted parameters at different β are the same at any one value of a_0. Indeed, when $\bar{E}\,\beta^2 a_0^2/z^2$ is plotted against t/a_0, as in Figure 4, the curves lie atop one another, except as affected by τ.

The essential conclusions to be summarized from these calculations are: 1) sites for which $t/a_0 < 1$ experience a dose which varies as $z^2\beta^{-2}t/a_0^{-2}$, while 2) sites for which $t/a_0 > 3$ experience a dose which varies as $z^2\beta^{-2}t^{-2}$.

We repeat these results for emphasis: when an ion passes at a distance of 3 or more site radii from the

Figure 3. The mean dose $\bar{E}$ deposited by secondary electrons (delta-rays) in a short cylinder of radius a_0, whose axis is parallel to and at distance t from the path of an ion of effective charge number z, moving at relative speed β, varies as a_0^{-2} when $t/a_0 < 1$, and is independent of a_0 when $t/a_0 > 3$, so long as both a_0 and t are smaller than τ, the greatest radial distance to which delta-rays penetrate. The dose always varies as z^2/β^2.

Figure 4. Except as affected by the relation of a_0 to τ, the greatest radial distance to which delta-rays penetrate, the mean dose $\bar{E}$ in a short cylinder whose axis is parallel to the ion's path is given by a single functional form, for all a_0, z, and β, when $\bar{E}\,\beta^2 a_0^2/z^2$ is plotted against t/a_0.

center of a site, the dose is independent of the radius of the site, and the point target approximation is valid; when an ion passes through a sensitive site, the dose to the site varies inversely with the square of the radius of the site. In all cases the dose varies as z^2/β^2.

Let us discuss track structure in a language appropriate to the appearance of particle tracks in emulsion, as shown in Figure 2, from the theory represented in Equation (2) and in Figure 4. We clearly must exclude from the discussion tracks formed in a detector whose sensitive elements are other than near spherical,

particularly when the bombardments are in the grain count regime, as is the case in the bombardment of tobacco mosaic virus with 4 MeV deuterons.[16]

If we draw a horizontal line on Figure 4, at $D_\gamma^{37}\beta^2 a_0^2 z^{-2}$, we can understand track structure from the position of the line relative to the curve. If the line lies above the "hat" of the curve, at 2.2×10^{-7} erg/cm, the quantity $\bar{E}/D_\gamma^{37} < 1$ for all sensitive sites, including those through which the ion passes. The probability for activation of any site, including those through which the ion passes, is less than 0.63, and the track is gapped and grainy. The higher the line, the more open the track. This describes the grain-count regime. Note that the position of the line relative to the curve depends both on the properties of the bombarding ion and those of the detector. If the line lies below 10^{-8} erg/cm, the track is fully closed along the ion's path, and sensitive
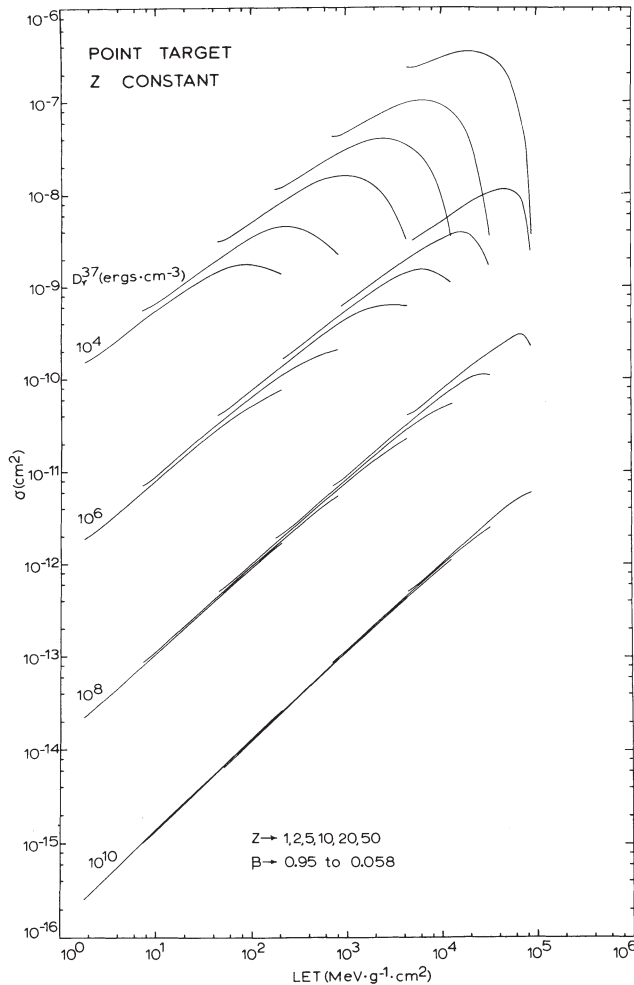
Figure 5. Theoretical values of the cross-section, σ, for the heavy ion activation of detectors for which $D_\gamma^{37} = 10^4$, 10^6, 10^8, and 10^{10} erg/cm³, are shown as a function of the stopping power (LET) of the bombarding ion. All curves are calculated in the point-target approximation. The 6 curves of each group are (left to right) $Z = 1, 2, 5, 10, 20$, and 50; and with points on each curve (right to left) for $\beta = 0.058, 0.145, 0.315, 0.52, 0.72$, and 0.95. The curves are here plotted with Z held fixed and with β varying along each curve.
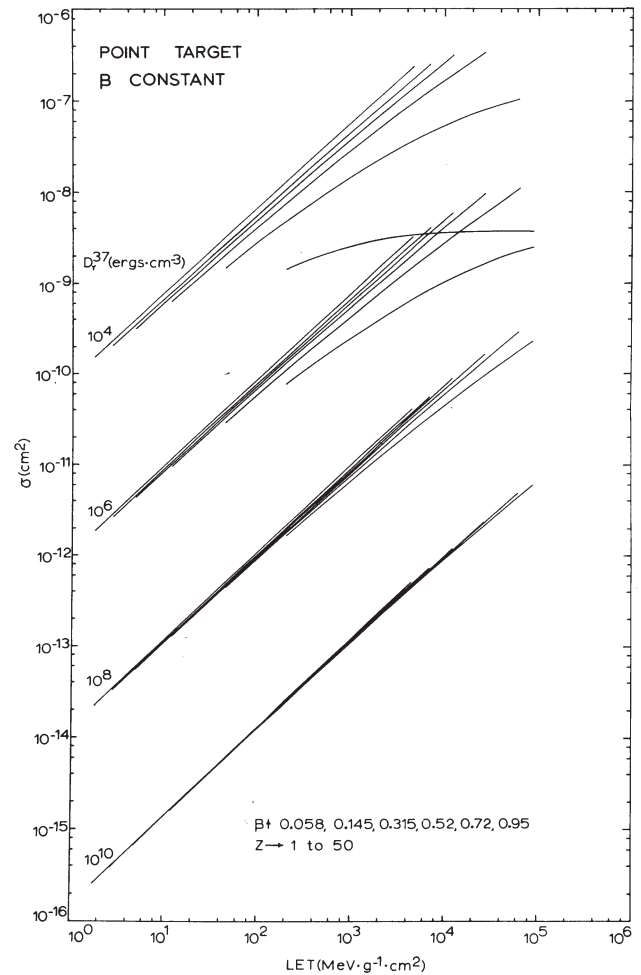
Figure 6. σ vs LET. Point-target. β constant. See caption to Figure 5.

sites at distances several times a_0 from the ion's path may be fully activated. This is the track-width regime, where the track has a cross-sectional area greater than the area of a sensitive site, and limited only by the distance beyond which no energy is deposited by delta-rays. An interaction which lies in the trackwidth regime of a sensitive detector may lie in the grain-count regime of an insensitive detector. Nevertheless, to repeat what has already been said, there are equal contributions to the activation in equal decade intervals in t, from the "track edge" to distances approaching τ.

In the present investigation we are concerned with detecting systems in which the details of the structure of an individual track are not resolvable. The detectors are sometimes thin enough for track segment analysis. In other cases we deal with stopping particles. It is sometimes convenient to examine the results obtained for particles of a single value of Z at different speeds. At other times the data are obtained with different Z, but a constant speed. The experimental data are most often plotted as a function of the track segment LET,

or the initial value of the LET of the incident particle. Sometimes we find the data for stopping particles plotted as a function of the initial kinetic energy of the bombarding particle. We have tried to follow the general practice in plotting the calculated response curves.

The theoretical results are displayed in a series of graphs. In Figures 5–10 we plot σ, k, and RBE, for detectors for which $D_\gamma^{37} = 10^4$, 10^6, 10^8, and 10^{10} erg/cm^3, as a function of LET, for ions for which Z = 1, 2, 5, 10, 20, and 50, at β = 0.058, 0.145, 0.315, 0.52, 0.72, and 0.95, plotted with Z held constant and again with β held constant. We repeat the calculations for stopping particles, showing $\overline{\sigma}R$ and $\overline{k}$, first at constant Z and then at constant β, in Figures 11–14. All of Figures 5–14 are calculated in the point-target approximation. We show the difference between the point-target and extended-target calculations for several bombarding ions at values of a_0 such that the calculated cross-section passes from below the geometrical cross-section to above it, from the grain-count to the track-width regime, in Figures 15 and 16. Note that the point-target approxi-
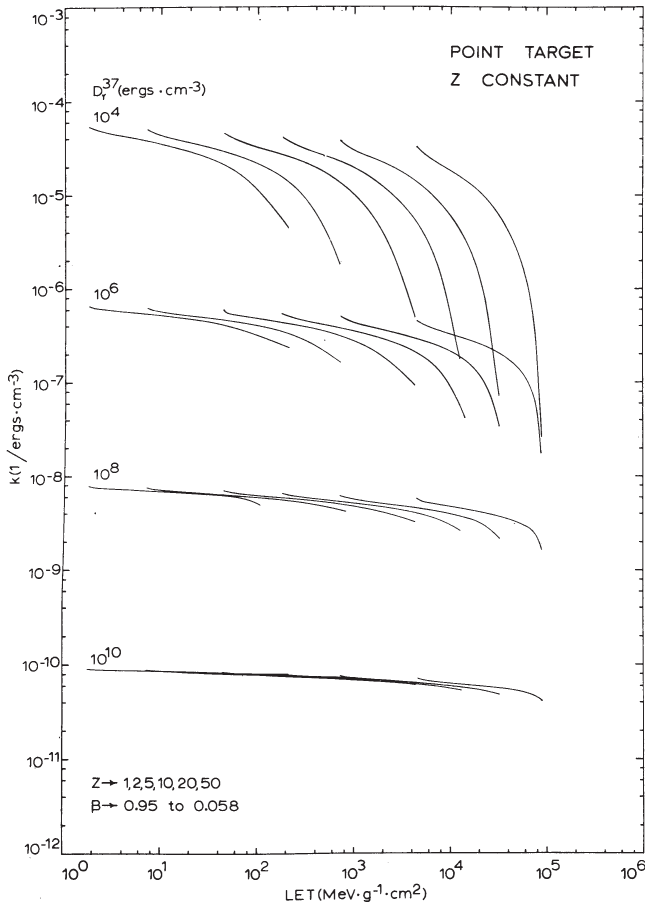
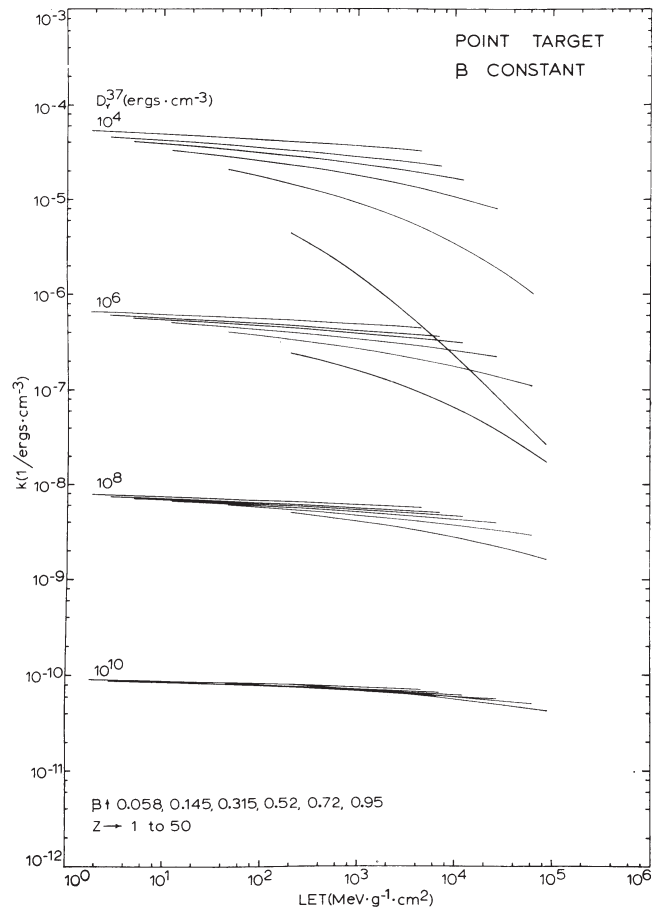**Figure 7.** k vs LET. Point-target. Z constant. See caption to Figure 5.

Figure 8. k vs LET. Point-target. β constant. See caption to Figure 5.

mation underestimates the cross-section, in the grain-count regime, and that there is no evidence of a plateau, or a saturation value of the cross-section, except as associated with τ.

The specific detector with which a particular set of response curves is to be associated is shown in Figure 1. Except at the highest values of D_γ^{37}, the response of 1-hit detectors is non-linear, and σ is a multiple valued function of LET, and becomes more acutely so with increasing detector sensitivity. Detector non-linearity and multiple valuedness may serve a useful purpose, in that one can combine sensitive and insensitive detectors to yield knowledge of Z and β of a particle suf-

ficiently energetic to pass through an adjacent pair of detecting elements. Such a system might provide useful information about the very heavy cosmic rays, for example.

In succeeding sections we make specific application of the theory to different detecting systems, shown here to have common characteristics.

In view of the apparent universal applicability of the delta-ray theory of track structure to detecting systems, we repeat its fundamental hypothesis: that the response of a detector to heavy ions may be found from knowledge of the local dose distribution about the ion's path from secondary electrons, and from knowledge of the
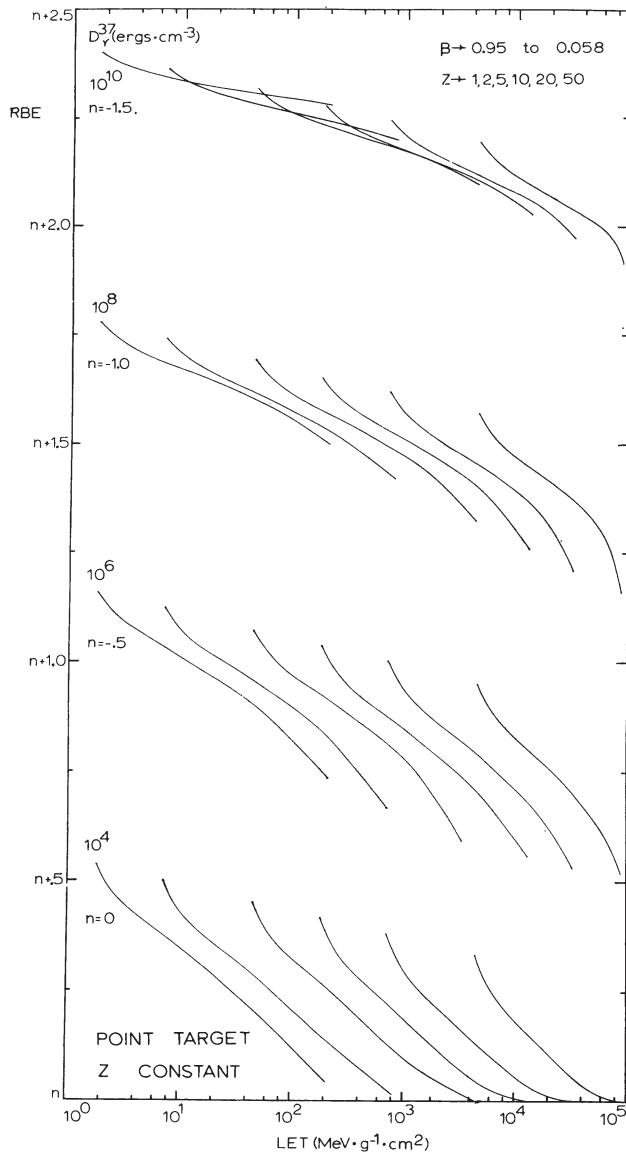
Figure 9. RBE vs LET. Point-target. Z constant. See caption to Figure 5. The quantity n is a vertical displacement parameter.
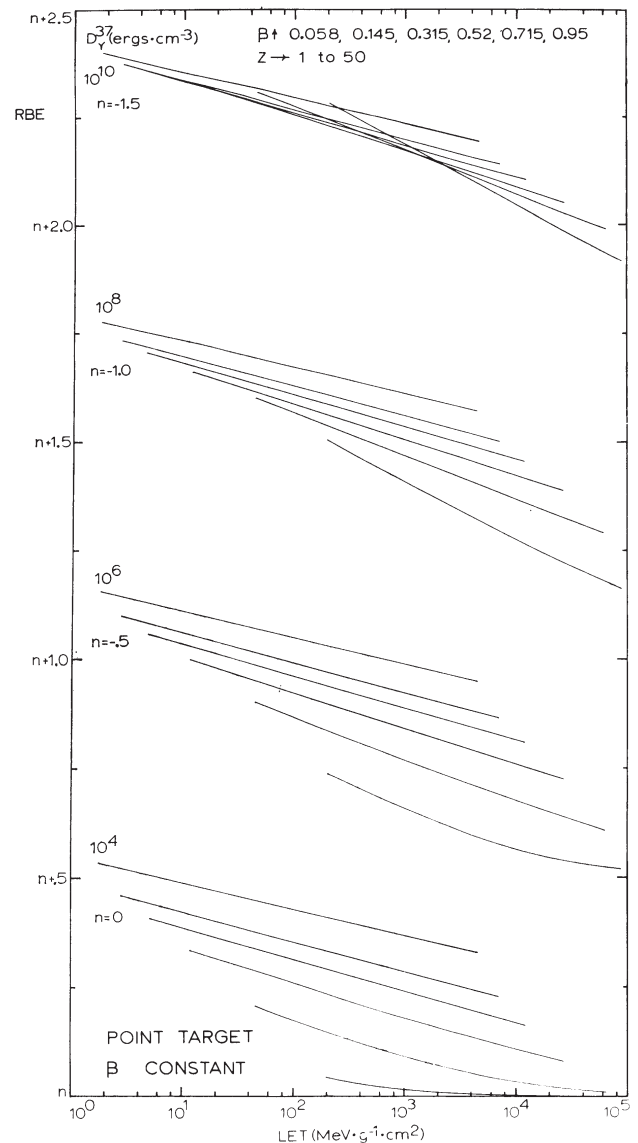
Figure 10. RBE vs LET. Point-target. β constant. See caption to Figure 9.

geometry of its sensitive elements and the detector's to gamma-rays. It is an important subsidiary result that there are many 1-hit detectors, whose response to both gamma-rays and heavy ions may be computed from two parameters — $D_\gamma{}^{37}$ and a_0. It is these parameters, and specifically their numerical value, that the theory of any particular detector must seek to explain.
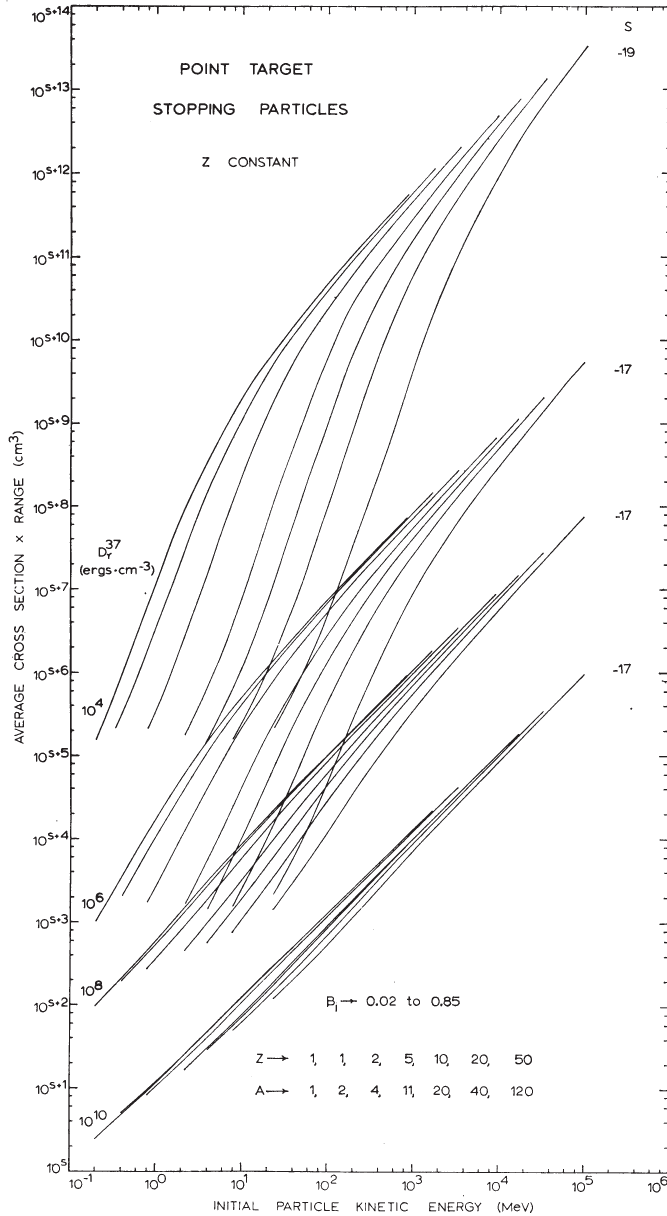
3. Solid state dosimeters: glass and LiF

Tochilin and co-workers [17,19] have shown that the response of the silver activated phosphate glass dosimeter and the TLD 100 LiF thermoluminescent dosimeter declines with an increase in the initial values of the LET of the bombarding particles which stop in the detector. By fitting calculated curves, in the point target approximation, to experimental data, we find that $D_\gamma{}^{37}$ = 3 × 10⁶ erg/cm³ for the glass dosimeter, as shown in

Figure 11. Theoretical values of the product of the average cross-section, $\bar\sigma$, by the range, R, of stopping particles, are plotted against the initial kinetic energy, T_i, of the incident particle. Calculations are in the point-target approximation, for a series of values of Z and β_i, and are plotted here with Z held constant and the initial value of the particle speed, β_i, varying along each curve. Note that in this presentation the response of protons is different from that of deuterons, with increasing separation of the proton and deuteron curves as the value of $D_\gamma{}^{37}$ for the detector decreases.

Figure 12. $\bar\sigma R$ vs T_i. β_i constant. Point-target. See Figure 11.

Figure 13. $\bar{k}$ vs. $\mathrm{LET_{initial}}$. Point-target. Z constant. See Figure 11.

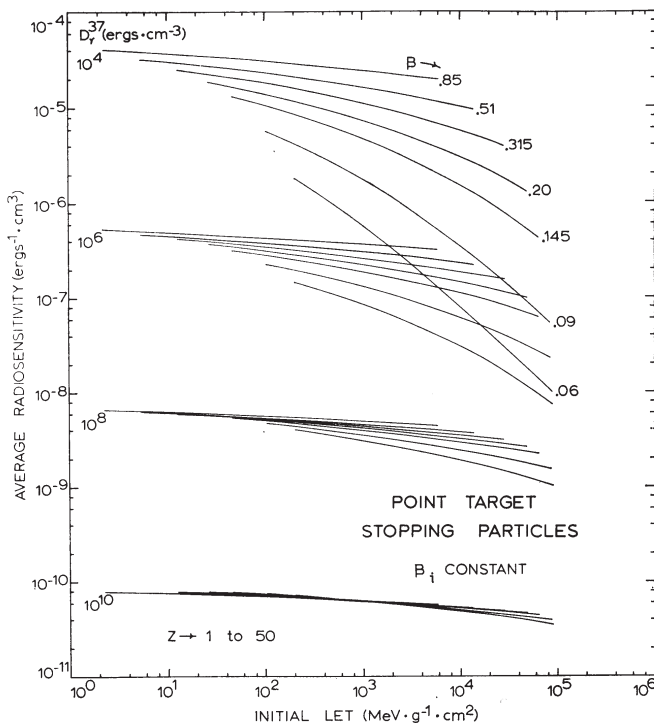**Figure 14.** k vs $\mathrm{LET_{initial}}$. β_i constant. Point-target. See Figure 11.

Figure 17, and that $D_\gamma^{37} = 10^7$ erg/cm³ for the LiF dosimeter, as shown in Figure 18. Scale factors by which the calculated values of the average radiosensitivity, $\bar{k}$, are converted to relative response are shown in the figure.

From the quality of the fit of the data to the fitted theory, even at low LET, we estimate that $a_0 < 10$ Å for each of these dosimeters.

Note that we here predict the gamma-ray dose-response relation from heavy-ion data.
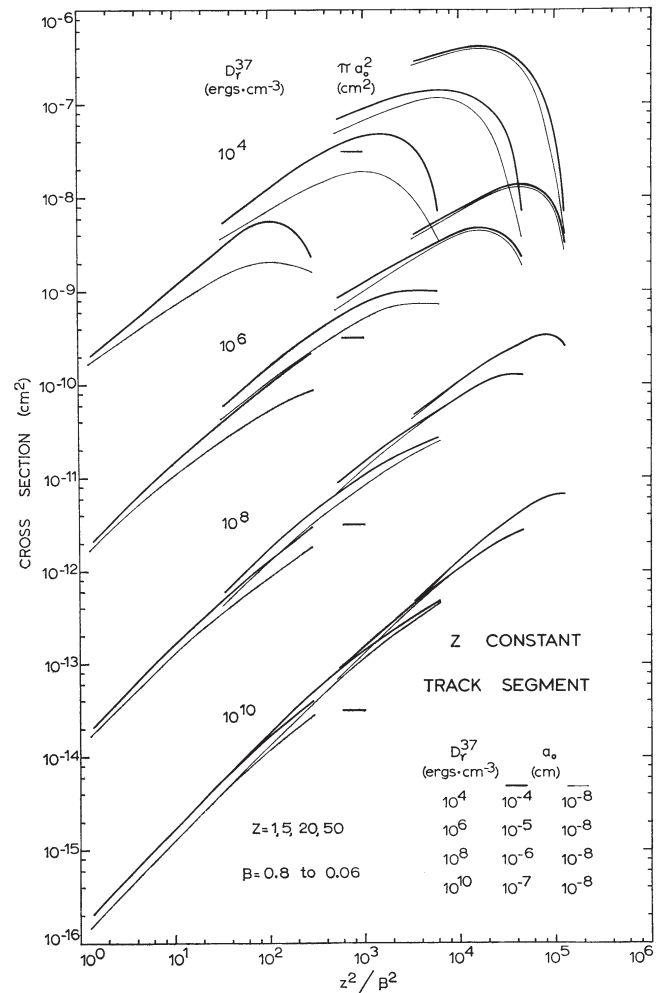
Figure 15. Theoretical values of the activation cross-section, σ, from extended-target calculations, are compared to point-target results. Values of a_0 and D_γ^{37} have been selected which yield cross-sections on either side of the geometric cross-section, πa_0^2, for the span of values of Z and β used in these graphs. Note: 1) that there is neither saturation, nor the suggestion of a plateau, near the geometric cross-section, and 2) that the point-target approximation (here calculated for $a_0 = 1$ Å) generally underestimates the cross-section in the grain-count regime, where $t/a_0 < 3$, or where $\sigma < 9\pi a_0^2$. Where $a_0 = 10^{-4}$ cm, problems associated with the range of the most energetic delta-ray make their appearance, as indicated in Figure 4. Z constant vs z^2/β^2.

4. Solid biological substances

In extension of earlier work on the theory of RBE for the heavy ion inactivation of dry enzymes and viruses,[6] we plot a raster of theoretical curves giving the inactivation cross-section for track segment bombardments, calculated in the point-target approximation, as a function of the stopping power (LET) of the bombarding ion (at 10 MeV/amu), for a series of values of D_γ^{37} in Figure 19.

Experimental data for different enzymes and viruses, from the heavy ion linear accelerators at Yale (Y) and Berkeley (B) are superimposed on the raster of theoretical lines.

In a table at the lower right hand corner of the figure, we give values of D_{exp}^{37}, determined experimentally with X-rays or gamma-rays, except where indicated by an asterisk, where the data arise from proton bombardment at 10 MeV/amu. We also show values of D^{37} which we assign from the position of the experimental cross-sections on the theoretical raster, which we label D_{th}^{37}. We are uncertain of the significance of discrepancies between these values, for there may be a contribution from dosimetry differences between apparatus measuring heavy ion dosimetry, and that used for gamma-ray dosimetry. The smallest discrepancies are associated with the cases where all dosimetry was with a single apparatus, as indicated by the asterisks.
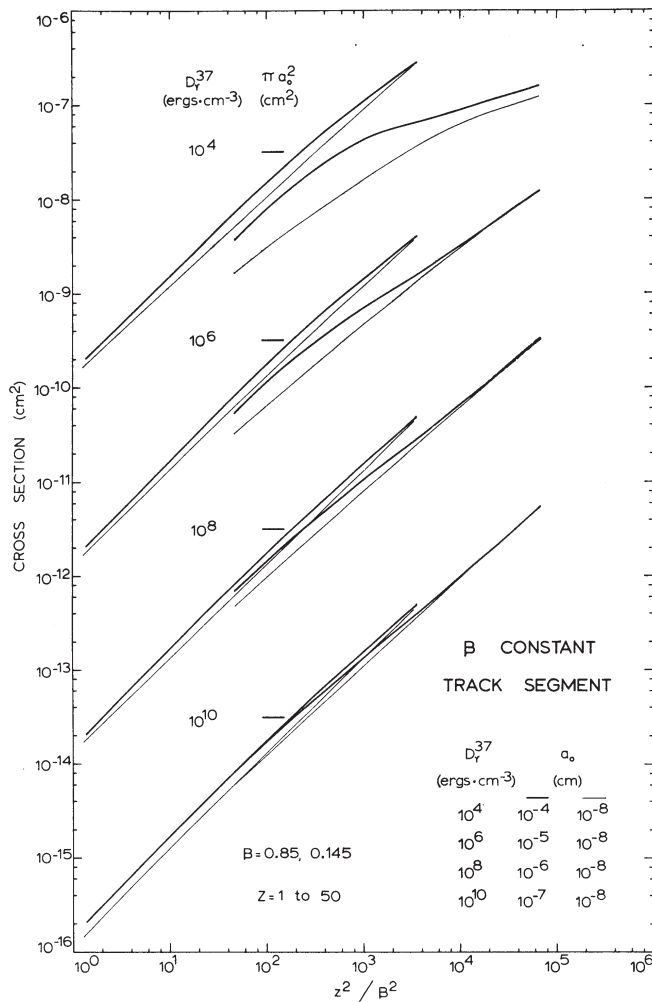
There are some other inconsistencies. For example, cross-sections for ΦX-174 phage lie on the raster in such a position that we would expect D_γ^{37} for this material to be about 2 times greater than the value of D_γ^{37} for T-1 phage, yet the two values are comparable. There are discrepancies in the measured cross-sections for Typsin, as between Yale and Berkeley measurements.

Aside from these minor discrepancies and inconsistencies, we find that the agreement between theory and experiment is excellent, and show, in Figure 20, exper-
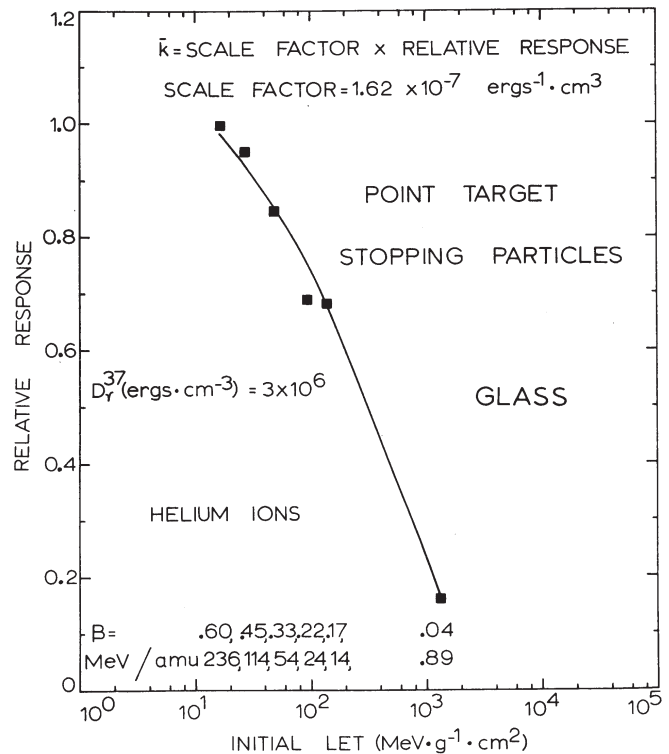
Figure 16. σ vs z^2/β^2. β constant. See Figure 15.

Figure 17. Relative response of the silver activated phosphate glass dosimeter, from Tochilin and co-workers,[17,19] as a function of the initial values of the stopping power (LET) of the bombarding helium ions. Theoretical values of $\bar{k}$ for these bombardments, calculated from the best fitting value of D_γ^{37}, are converted to relative response by a multiplicative scale factor. We find $D_\gamma^{37} = 3 \times 10^6$ erg/cm^3, for this detector. The value of the relative speed (β) and the initial energy of the bombarding ions are shown directly beneath each plotted point.

imental cross-section data for these substances plotted over the theoretical relationships calculated from the value of $D_{th}{}^{37}$. A line joins calculated values of the cross-section of all bombardments at 10 MeV/amu, while other calculated values at different ion speeds are plotted as + signs, with experimental values lying closeby. There is no evidence from these data of a plateau or a saturation value of the cross-section, in agreement with the present theory.

Data on Trypson (B), DNAase, and Lysozyme are from Brustad.[20] References to other data are given in Butts and Katz.[6]

According to Hendriksen,[21] the yield of secondary radicals in several solid biological substances, bombarded with 6.5 MeV electrons, and with heavy ions up to Z= 18 at 10.4 MeV/amu, declines with an increase in the stopping power of the particle responsible for radical production. Samples used by Hendriksen ranged from about 20 to 50 mg/cm², too thick for track segment assumptions, and too thin to stop all bombarding ions. We have attempted to bracket the data between
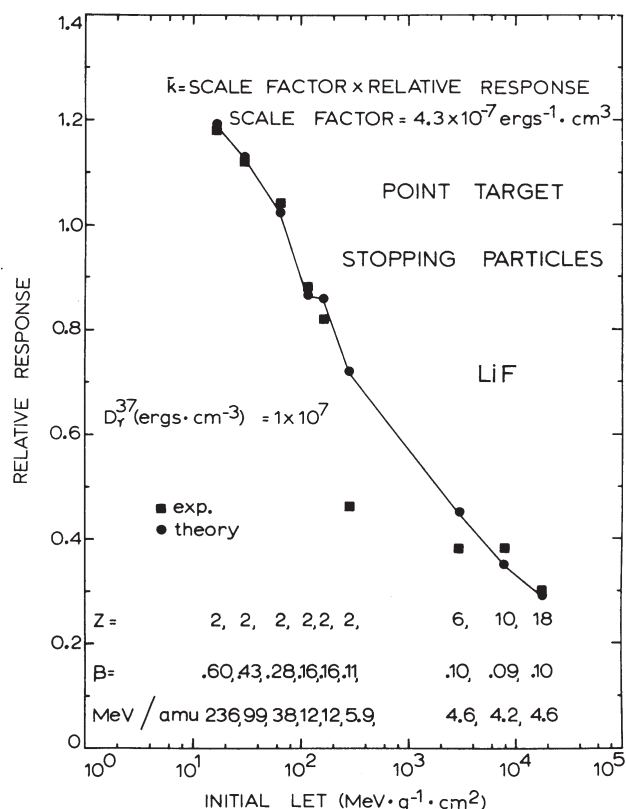
theoretical calculations for segment and for stopping particles. In general, the heavier particles were stopped in the specimen.

Our best fit of these data is shown in Figures 21-23, where the data are plotted over the best fitting calculations of $\bar{k}$, in the point-target approximation, with the multiplicative factor connecting $\bar{k}$ to radical yield shown in each case. Fitted values of $D_\gamma{}^{37}$ are shown for each substance. In all cases, experimental values of the yield for electron bombardment are shown by asterisks
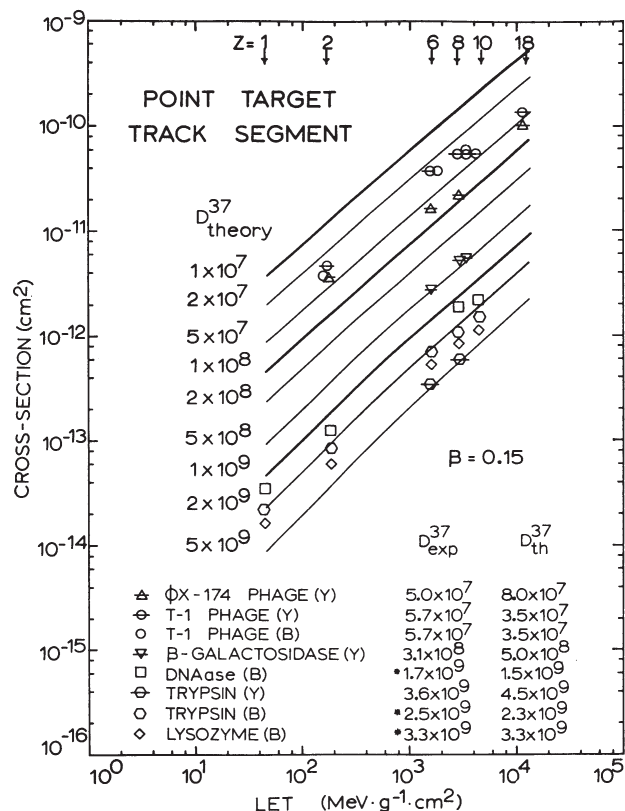

Figure 19. Theoretical values of the cross-section, in the point-target approximation, are plotted as a function of LET for ions at $\beta = 0.145$, and $D_\gamma{}^{37}$ ranging from 10^7 to 5×10^9 erg/cm³. Measured values of the inactivation cross-sections of some dry enzymes and viruses, as obtained at the Yale (Y) and Berkeley (B) heavy ion linear accelerators, are superimposed on the raster of theoretical lines. We emphasize that the points arise from experiment, with no fitting, while the lines arise from theory. Shown at the top of the figure are the values of Z giving the indicated LET at $\beta = 0.145$. In the table at the lower right hand corner of the figure, experimental values of $D_\gamma{}^{37}$ are quoted. Where these values are not available, as indicated by asterisks, the quoted values are the values of $D_p{}^{37}$, the D^{37} dose obtained with protons at 10 MeV. In the table we give values of the D^{37} dose assigned from the position of the experimental cross-sections on the theoretical raster, identified as $D_{th}{}^{37}$. Discrepancies between $D_{exp}{}^{37}$ and $D_{th}{}^{37}$ may arise from experimental differences in gamma-ray and ion dosimetry. Data for DNAase, Trypsin (B), and Lysozyme are from Brustad.[20] Other references are given in Reference 6.

Figure 18. Relative response of the TLD-100 LiF thermoluminescent dosimeter, as a function of LET, from Tochilin and co-workers.[17,18] For this detector, $D_\gamma{}^{37} = 10^7$ erg/cm³. The values of the atomic number, relative speed (β), and initial energy of the bombarding ions are shown directly beneath the plotted points.

alongside the radical yield axis. The curves are plotted against the initial values of z^2/β^2 of the bombarding ion, rather than LET, to avoid problems arising from small differences in density.

Hendriksen [21] noted that graphs of the relative yield of secondary radicals against LET were similar in shape to plots of the radiosensitivity (to inactivation), from the data of Brustad,[20] and concluded, from this evidence, that secondary radicals are somehow involved in the sequence of reactions leading to loss in enzyme activity.

Our conclusions differ from those of Hendriksen. We point out that the shapes of these curves, of $\bar{k}$ (for the thick specimens of Henriksen) or of k (for the thin specimens of Brustad), when plotted against LET, is characteristic of the 1-hit process. The relevent datum
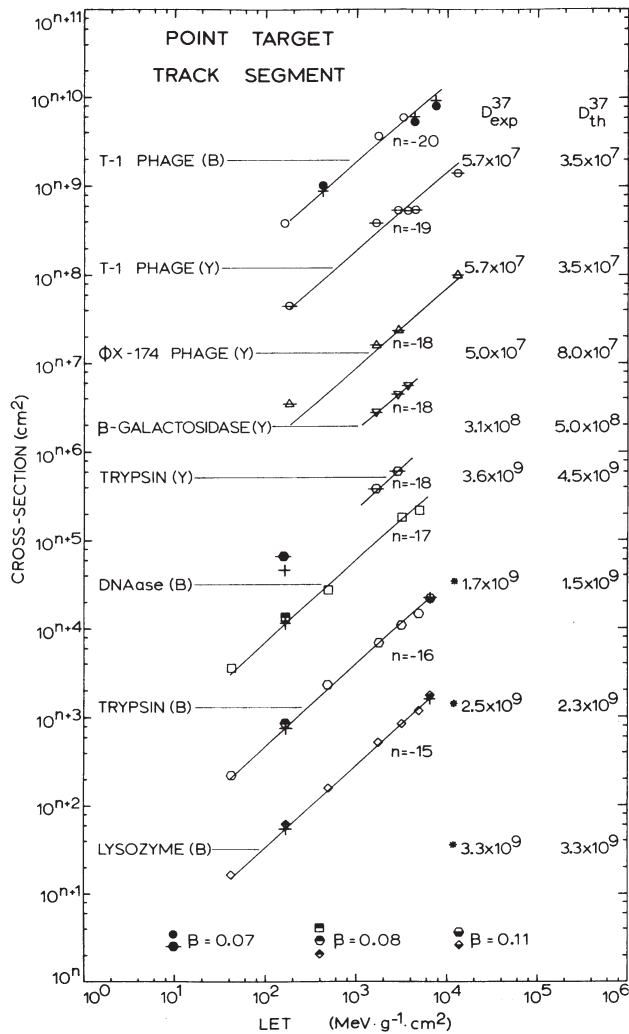
Figure 20. Published data on the heavy ion inactivation of dry enzymes and viruses are plotted against the LET of the bombarding ion, for comparison with theoretical values of σ, calculated from D_{th}^{37} (from Figure 19) in the point-target approximation. Lines connect values calculated for ions at 10 MeV/amu ($\beta = 0.145$). Other calculated cross-sections are shown as + signs, to be compared to adjacent experimental points. The data and theoretical curves for the different substances are nested by use of a vertical separation parameter, n.
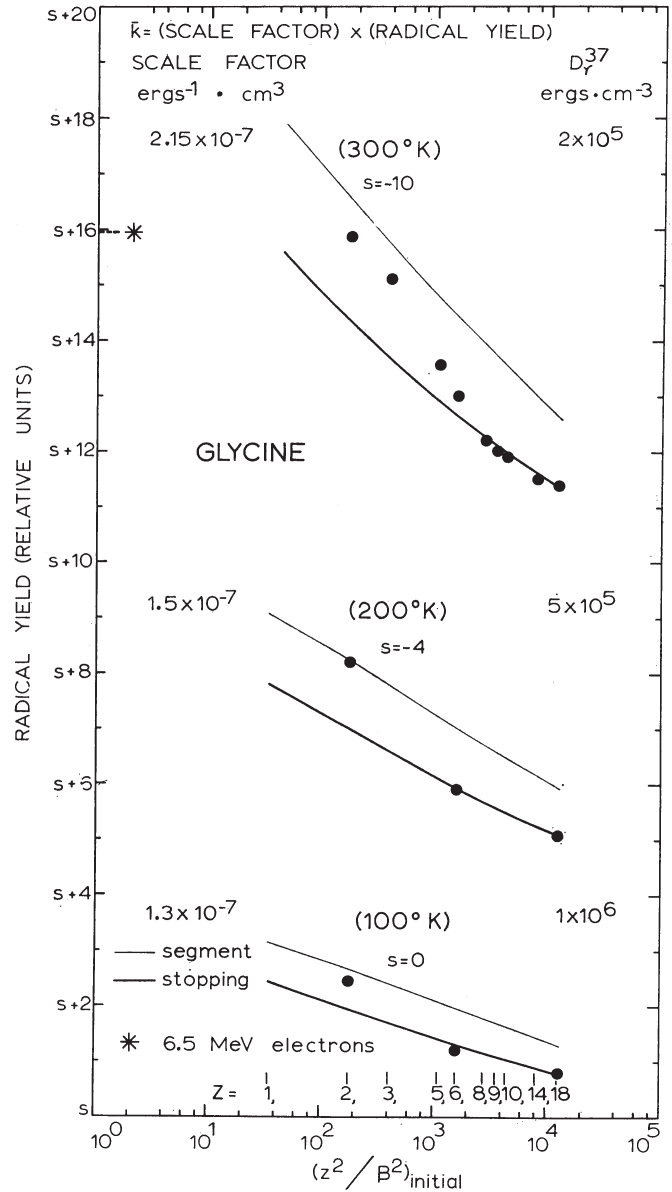
Figure 21. Relative radical yields in Glycine, at 100, 200, and 300 K, when bombarded with electrons at 6.5 MeV, and ions at 10 MeV/amu, are compared to theoretical values of $\bar{k}$, at the indicated values of D_γ^{37}, by use of a multiplicative factor. Curves are separated by use of a vertical displacement parameter s. Point target calculations are shown, for thin specimens (segment) and thick specimens (stopping), since the lighter ions used in the experimental investigation, by Henriksen,[20] penetrated the specimens. Asterisks along the vertical axis give the relative yield for 6.5 MeV electrons.

is not the curve shape when normalized on a linear plot but rather the value of D_γ^{37}, which is 3×10^9 erg/cm^3 for the inactivation of Trypsin, and which is 10^7 erg/cm^3 for radical formation. We conclude that these data do not demonstrate that the inactivation of Trypsin arises from the production of radicals.

We wish to call attention to a very interesting application of esr measurements, by Henriksen, Horan, and Snipes,[22] to test the thermal spike mode of tracks structure. Their experiment is based on the properties of DL-Valine, in which radicals formed at 77 K are converted to secondary radicals on heat treatment. According to their calculations, the thermal spike model demands that there be a measurable conversion of the primary radical to a secondary radical form in this substance when bombarded with heavy ions. Yet no difference is observed in the esr spectrum, as between electron and ^{40}Ar bombardment. It is their conclusion that the thermal spike model is inapplicable to radical formation.

This is the only clear experimental test known to us of the thermal spike model of track structure. We should like to make the additional point that this experimental finding is in complete agreement with the present theory, which holds that track effects arise principally from secondary electrons. We expect no qualitative differences to arise from electron and from Ar bombardment.

The experiment further confirms our view that there is no present basis for assuming that phenomena taking place in the "core" of a track are different from those that take place in the delta-ray "cloud." Indeed, there seems to be no basis other than one of perception, for the belief that track core is a meaningful concept.

5. Organic scintillators

Plots of the response of solid and liquid organic scintillators, against the LET of the incident particle, display non-linearities and multiple-valuedness, parallel to that observed for NaI(Tl) and CsI(Tl).[23]

We are able only to make a partical analysis of the response of organic scintillators, for these detectors
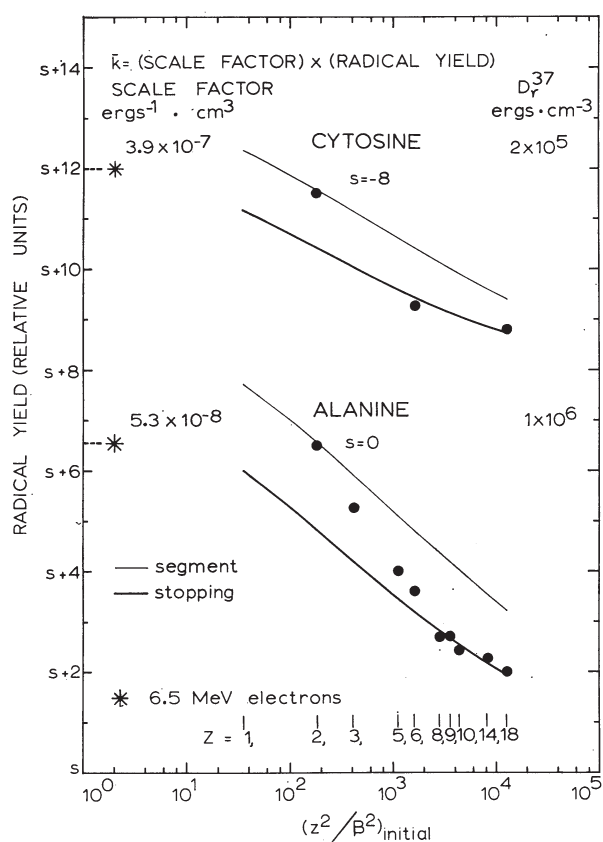
Figure 22. Relative radical yields in Cytosine and Alanine, as compared to fitted theory. See Figure 21.
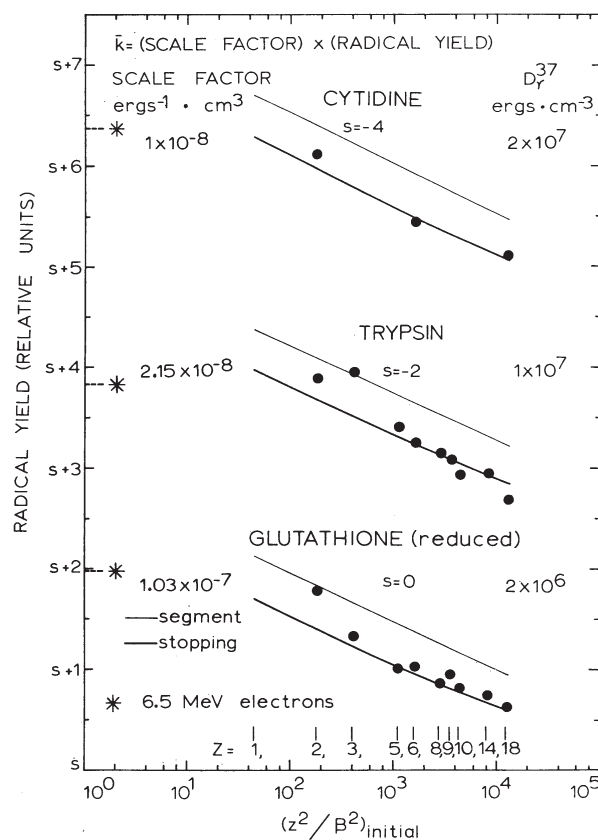
Figure 23. Relative radical yields in Cytadine, Trypsin, and Glutathione (reduced), as compared to fitted theory. See Figure 21. More than two orders of magnitude separate the value of D_γ^{37} for radical formation in Trypsin from the value of D_γ^{37} for inactivation, as shown in Figures 19 and 20.

have been studied principally with electrons, protons, and deuterons, with very little information available regarding their response to energetic heavy ions. The available data give the relative pulse height as a function of the initial kinetic energy of a particle which stops in the detector. These data are compared to theoretical plots of $\overline{\sigma}R$ vs T_i, as in Figures 11 and 12. The experimental plots are sometimes differentiated graphically to obtain track segment information, which we compare to theoretical plots of σ vs L, as shown in Figures 5 and 6, as we have done earlier for NaI(Tl).[5]

Experimental data giving the relative pulse height observed in a mineral oil based liquid scintillator sensitized with PPO (2,5 diphenyl oxazole), with proton and deuteron bombardment to 200 MeV, are given by Webb, Hauser and Mischke.[24] In Figure 24 we plot $(\overline{\sigma}R$ vs T_i for protons and deuterons, calculated in the point target approximation, for $D_\gamma{}^{37} = 10^4$ erg/cm³, divided by the indicated scale factor, so that the theoretical curve may be compared directly to experimental data.
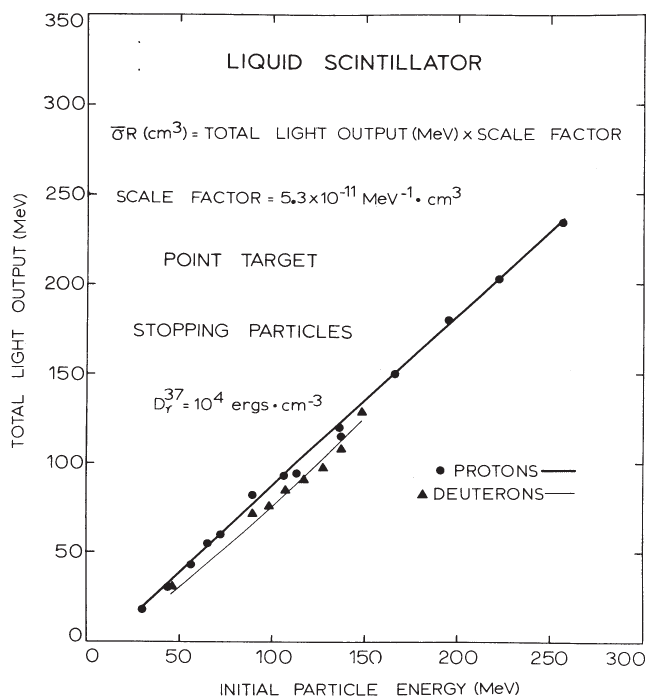

Figure 24. The relative light output of a mineral oil base liquid scintillator sensitized with PPO, at the Princeton-Penn accelerator, when bombarded with energetic protons and deuterons, as a function of the initial kinetic energy of these particles. Data are compared to curves giving $\overline{\sigma}R$ for $D_\gamma{}^{37} = 10^4$ erg/cm³ by use of a multiplicative scale factor. The relative light output is measured in units of the electron energy, in MeV, giving the observed light output with heavy ions. Data are from Webb, Hauser and Mischke.[24]

We have referred earlier to the use of a graph of pulse height versus PPO concentration in a solution of xylene and p terphenyl to estimate that $a_0 = 150$ Å for this scintillator. If we take a_0 to have the same value for the mineral oil based scintillator discussed above, we find the proton and deuteron bombardments to be in the track width regime of this detector, so that the point target evaluation of $D_\gamma{}^{37}$ is valid. These results imply that the response of the Princeton-Penn liquid scintillator may be predicted from Figures 5–14, for the ions and energies plotted there.

Even fewer data are available for the variation of response with LET in solid organic scintillators. From data on the response of anthracene, stilbene, NE 102, NE 213, NE 230, and Pilot B solid organic scintillators to stopping protons or deuterons of initial energy below 15 MeV, as compared to point target calculations, we find that an upper limit to the value of $D_\gamma{}^{37}$ for these detectors is approximately 10^6 erg/cm³, all these detectors being fairly closely grouped.

We have no information on which to base an evaluation of a_0, and do not know whether these bombardments are in the grain-count or track-width regime for these detectors. Since point target calculations underestimate the value of $D_\gamma{}^{37}$ in the grain-count regime, it is possible that the value of $D_\gamma{}^{37}$ estimated by fitting the point target calculations to proton data results in an overestimate.

6. The ferrous sulfate (Fricke) dosimeter

Calculated values of the mean radiosensitivity, $\overline{k}$, of stopping deuteron, helium, and carbon ions are plotted as a function of the initial values of the LET of the bombarding ions, in Figure 26. The calculations are made in the point-target approximation, and for $a_0 = 60$ Å, for $D_\gamma{}^{37}$ from 10^7 to 10^9 erg/cm³.

Data for the dosimeter yield, when irradiated with X-rays, gamma-rays, deuteron, helium, and carbon ions of different energies, from different investigators, are superimposed on the calculated curves by means of the multiplicative scale factors shown on the figure.

Theoretical values of k_γ are shown by an asterisk alongside the radiosensitivity axis, for comparison to the experimental values which are plotted at values of LET assigned by the original investigator.

As already discussed, the point-target model describes the relationship between k_γ and $\overline{k}$ adequately, for bombardments in the track-width regime, but underestimates the detector response in the grain-count regime, as shown in Figure 26. At $D_\gamma{}^{37} = 5 \times 10^7$ erg/cm³, the asterisk representing k_γ is aligned with the
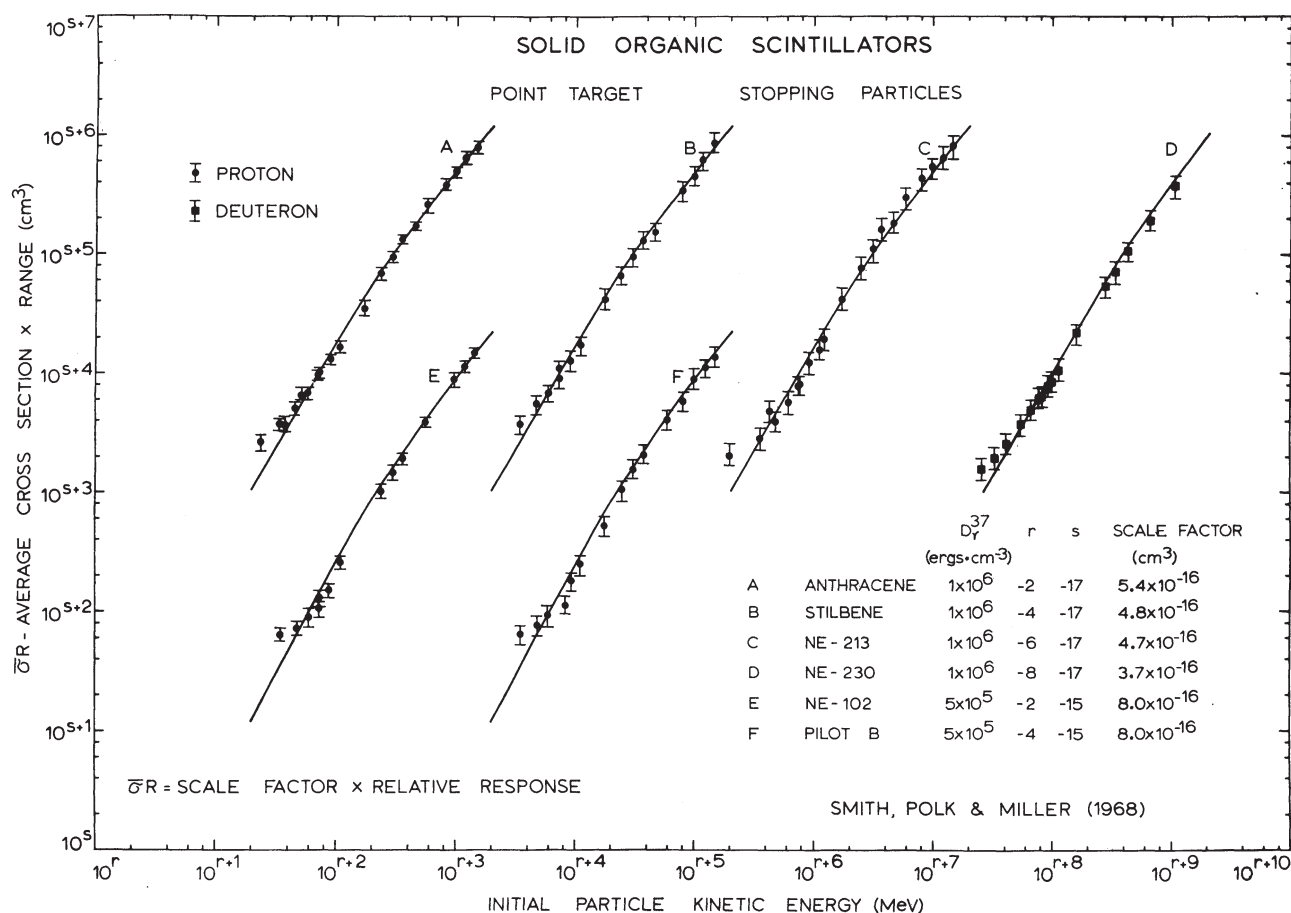
Figure 25. The relative light output from some solid scintillators, as a function of the initial kinetic energy of the incident proton. The data, from Smith, Polk and Miller,[25] are compared to the fitted theory.

gamma-ray data, and the light line, from point-target calculations, is fairly well aligned with the carbon data, but the light lines underestimate the deuteron and helium ion response. Overall agreement of theory and experiment is much better at $a_0 = 60$ Å, shown in heavy lines. The results for $a_0 = 60$ Å are replotted on a linear yield axis for clearer comparison with the data, in Figure 27.

Some of the data for the aerated dosimeter is available also, in the form of yield as a function of the initial kinetic energy of the bombarding ion, from Schuler[27] and from Schuler and Allen.[28] In Figure 28 we compare these data to curves calculated from the parameters indicated in Figure 26.

From Equation (11) and the parameters $D_\gamma^{37} = 5 \times 10^7$ erg/cm^3 and $a_0 = 60$ Å, evaluated in Figure 26, we calculate the yield of the aerated Fricke dosimeter to 14 MeV neutrons, making use of the initial energy spectrum of secondary charged particles in tissue, from Caswell,[29] as an approximation to the dosimeter solu-

tion. We find the ratio of the D^{37} dose for gamma-rays to the D^{37} dose for neutrons, D_N^{37}, to be $D_\gamma^{37}/D_N^{37} = 0.63$. Taking $G(Fe^{3+})$ to have the value 15.6/100 eV for gamma-rays, we find the value for 14 MeV neutrons to be 9.8/100 eV. This value is to be compared to a value of $11.5 \pm 1.8/100$ eV, reported by Axtmann and Licari, for 14.6 MeV neutrons incident on the aerated Fricke dosimeter.

The present model of radiation action in aqueous solutions makes it clear that the LET variation of the response of the Fricke dosimeter is a statistical phenomenon arising from the 1-hit character of its response and the spatial distribution of action events, as it is in scintillation counters [5] and other detectors, and that the chemical processes play themselves out in a way that is programmed by what happens in the sensitive volume. As in other detectors we are uncertain as to the details of the interactions represented by D_γ^{37}, and why water acts collectively over a volume element of radius 60 Å. These questions remain for further investigation.
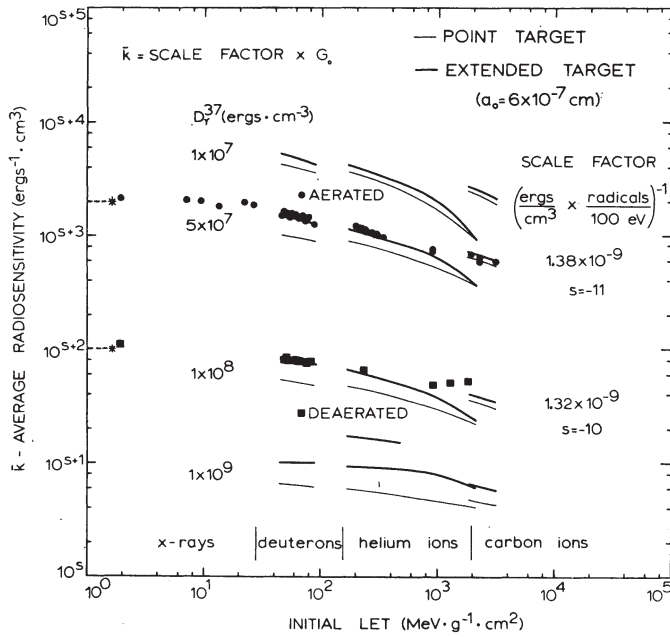
Figure 26. Data for the response of the Fricke dosimeter, in aerated and in deaerated solutions, given as a function of the initial value of the stopping power ($LET_{initial}$) of the bombarding ion, is compared to calculations made at several values of D_γ^{37}, in the point target approximation, and for $a_0 = 60$ Å. An asterisk alongside the radiosensitivity axis gives the value of the radiosensitivity for the best fitting theoretical curves. As indicated earlier, the point target approximation underestimates the response at low LET.
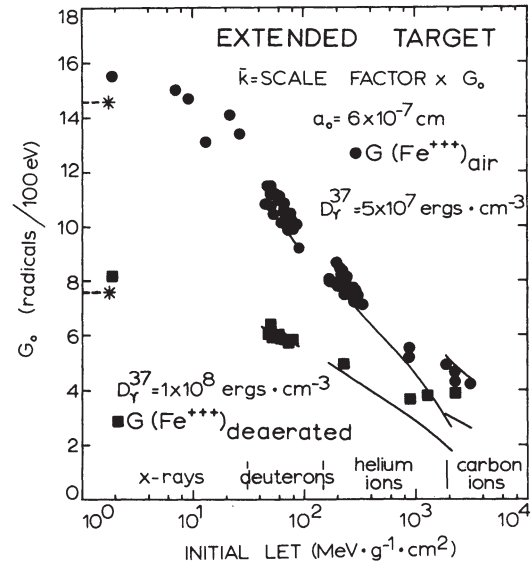

Figure 27. The data of Figure 26 and the calculated curves for $a_0 = 60$ Å are replotted on a linear G axis, because of the importance of the application of the present model to conceptual structures in radiochemistry.
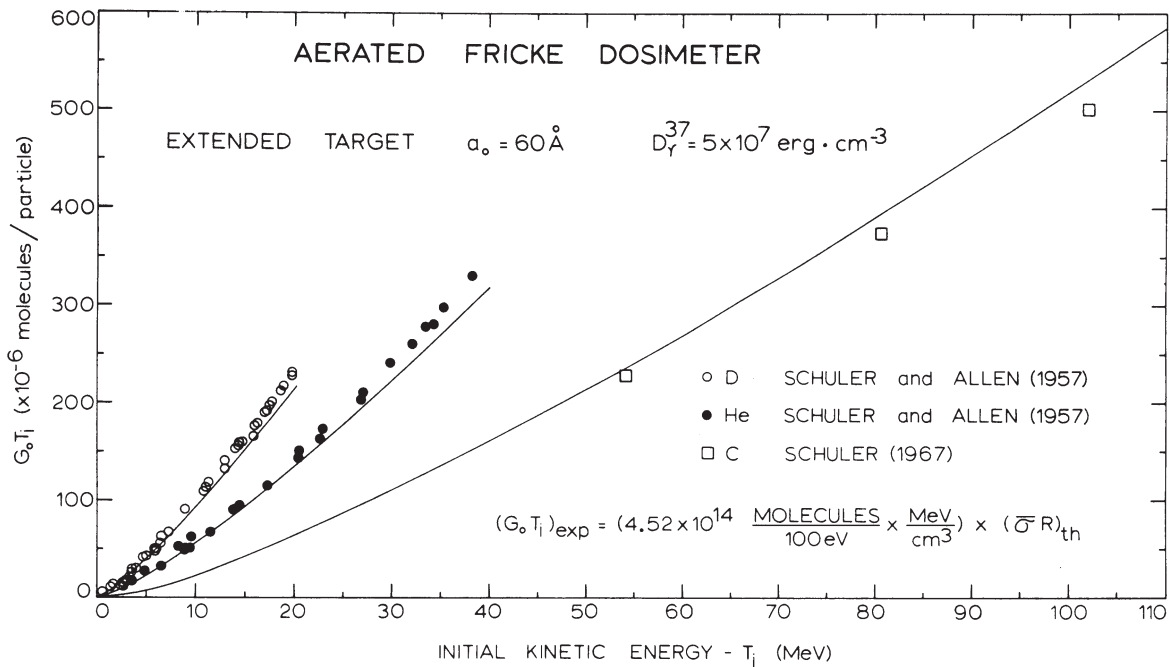

Figure 28. Some of the data of Figures 26 and 27 are available in the form of yield as a function of the initial kinetic energy of the bombarding ion. Using parameters evaluated by a criterion of best visual fit to the available data from all sources, as shown in Figure 26, we show calculated values of $\bar{\sigma}R$ plotted against T_i for stopping deuteron, helium, and carbon ions (converted to a relative yield scale by use of the scale factor of Figure 26), in comparison with the data of Schuler[27] and Schuler and Allen.[28] These response curves bear a strong resemblance to similar graphs arising from study of the response of scintillation counters.[23]

The present model offers a quantitative alternative to the spur-diffusion model of radiation action in chemical solutions by heavily ionizing particles, which is based on a rather detailed approximation to track structure, using such terms as spurs, blobs of different initial shapes, and short tracks, all rather arbitrarily defined, and distinguishing these from track-core; an array of diffusion constants; and of coupled partial differential equations.[26,31,33] In view of the present work, we question whether the complexity and detail of the spur-diffusion model is justified.

References

1) R. Katz, B. Ackerson, M. Homayoonfar, and S. C. Sharma, *Radiation Res.* **47** (1971) 407.

2) R. Katz and E. J. Kobetich, *Phys. Rev.* **170** (1968) 401.

3) R. Katz and E. J. Kobetich, *Phys. Rev.* **186** (1969) 344.

4) B. Ackerson, C. M. Sorensen, and R. Katz, *Nucl. Instr. and Meth.* **92** (1971) 81.

5) R. Katz and E. J. Kobetich, *Phys. Rev.* **170** (1968) 397.

6) J. J. Butts and R. Katz, *Radiation Res.* **30** (1967) 855.

7) C. P. Bean, M. V. Doyle, and G. Entine, *J. Appl. Phys.* **41** (1970) 1454.

8) H. Dertinger and H. Jung, *Molecular radiation biology* (Springer-Verlag, New York, 1970).

9) J. A. Harshaw, E. C. Stewart, and J. O. Hay, AEC Report NYO 1577 (1952) unpublished.

10) F. D. Brooks, in *Progress in nuclear physics,* vol. 5 (ed. O. R. Frisch; Pergamon Press, New York, 1956) p. 252.

11) R. Katz, in *Proc. 2nd Symp. Microdosimetry* (Stresa, Italy, 1969); Euratom EUR 4452 d-f-e (1969).

12) W. H. Barkas, *Nuclear research emulsions,* vol. 1 (Academic Press, New York, 1963).

13) J. F. Janni, Air Force Weapons Laboratory Technical Report no. AFWL-TR-65-150 (1956) unpublished.

14) L. C. Northcliffe and R. F. Schilling, *Nucl. Data Tables* **7** (1970) 233.

15) W. H. Barkas and M. J. Berger, NAS-NRC Publ. 1133; Nucl. Sci. Ser. Report no. 39 (1964) p. 103.

16) E. C. Pollard and G. F. Whitmore, *Science* **122** (1955) 335.

17) E. Tochilin and B. M. Shumway, in *Radiation dosimetry,* vol. III (eds. F. H. Attix and E. Tochilin; Academic Press, New York, 1969) p. 247.

18) C. L. Wingate, E. Tochilin, and N. Goldstein, in *Proc. Intern. Conf. Luminesence dosimetry* (Stanford, Calif., April 1967) p. 421.

19) E. Tochilin, N. Goldstein, J. T. Lyman, and W. G. Miller, U. S. Naval Radiological Defense Laboratory Report no. NRDL-TR-68-129 (San Francisco, 7 Nov. 1968) unpublished.

20) T. Brustad, *Radiation Res. Suppl.* **2** (1960) 65.

21) T. Henriksen, *Radiation Res.* **27** (1966) 676.

22) T. Henriksen, P. K. Horan, and W. Snipes, *Radiation Res.* **43** (1970) 1.

23) J. B. Birks, *The theory and practise of scintillation counting* (Pergamon Press, New York, 1964).

24) R. C. Webb, M. G. Hauser, and R. E. Mischke, *Nucl. Instr. and Meth.* **88** (1970) 227.

25) D. L. Smith, R. G. Polk, and T. G. Miller, *Nucl. Instr. and Meth.* **64** (1968) 157.

26) A. O. Allen, *The radiation chemistry of water and aqueous solutions* (Van Nostrand, New York, 1961).

27) R. H. Schuler, *J. Phys. Chem.* **71** (1967) 3712.

28) R. H. Schuler and A. O. Allen, *J. Am. Chem. Soc.* **63** (1959) 808.

29) R. S. Caswell, private communication (1971).

30) R. C. Axtmann and J. A. Licari, *Radiation Res.* **22** (1964) 511.

31) A. Mozumder, in *Advances in Radiation chemistry,* vol. 1 (eds. M. Burton and J. L. Magee; Wiley-Interscience, New York, 1969).

32) A. Kuppermann, in *Radiation research* (ed. G. Silini; North-Holland Publ. Co., Amsterdam, 1967).

33) A. Appleby and H. A. Schwartz, *J. Phys. Chem.* **731** (1969) 1937.